Comparison of monochromators for wavelength-modulated atomic absorption and emission spectrometry

ARTICLE *in* ANALYTICAL CHEMISTRY · MAY 1984

Impact Factor: 5.64 · DOI: 10.1021/ac00270a009

1 AUTHOR:

James Harnly
Agricultural Research Service
163 PUBLICATIONS **3,397** CITATIONS

SEE PROFILE

Theoretical Comparison of Monochromators for Wavelength-Modulated Atomic Absorption and Emission Spectrometry

James M. Harnly

Nutrient Composition Laboratory, Beltsville Human Nutrition Research Center, Agricultural Research Service, Science and Education, U.S. Department of Agriculture, Beltsville, Maryland 20705

Snelleman's equations for wavelength modulated continuum source atomic absorption spectrometry (WMCS-AAS) can be extended directly to wavelength modulated atomic emission spectrometry (WM-AES). The equations for the detection limit and the cathodic current are the same for WMCS-AAS and WM-AES when only the monochromator parameters are considered. The ideal monochromator (the best detection limit) possesses a short focal length, a high angular dispersion, a large grating area, and a large slit height. Within the constraints necessary to meet the underlying assumptions of Snelleman's equations, high and medium resolution monochromators give the best detection limits for WMCS-AAS. For WM-AES, however, low-resolution monochromators offer detection limits comparable to the more expensive, medium- and high-resolution monochromators.

Wavelength modulation has proven to be a valuable spectroscopic tool for discriminating against low frequency flicker noise and correcting for broad band spectral interferences. The use of wavelength modulation, or repetitive ac scanning, was first described by Snelleman (*1*). Wavelength modulation has been successfully used with continuum source atomic absorption spectrometry (WMCS-AAS) (*2–7*) and atomic emission spectrometry (WM-AES) (*8–15*) for both flame and furnace atomization. In the past 6 years a WMCS-AAS instrument has been developed with multielement capabilities and extended calibration ranges (*6*, *16*, *17*). It has been demonstrated that these same features can be realized for WM-AES (*18*).

Previously, dispersion devices for WMCS-AAS were selected for high resolution and not from careful consideration of Snelleman's equations. In the past 10 years, a high-resolution echelle spectrometer with the narrowest slit widths has been routinely used for WMCS-AAS to obtain the best resolution, analytical sensitivities, and calibration curve linearities. While the high angular dispersion of the echelle is in keeping with Snelleman's equations, the detection limits are not dependent on the resolution. With very small or very large slit parameters, deviations from Snelleman's model are observed which result in a degradation of the detection limits (*19*).

Snelleman did not derive equations to cover WM-AES. In practice, a wide variety of monochromators have been used with equal success. In one case, high resolution was found to reduce analytical curve linearities (*12*).

In this study, Snelleman's equations will be used to evaluate commercially available monochromators for WMCS-AAS and WM-AES on the basis of detection limits. Equations are derived for WM-AES comparable to those for WMCS-AAS. These equations are then simplified to only those parameters associated with the monochromator. Experimental data will be used to define those areas where the underlying assumptions of Snelleman's equations are not met. In this manner, the optical parameters can be limited so that a valid theoretical comparison of monochromators can be made.

THEORETICAL PARAMETERS

The same general logic for deriving the detection limits prevails for WMCS-AAS and WM-AES. For WMCS-AAS, the absorption signal must be large enough such that the decrease in intensity can be differentiated from the continuum source noise, whereas, for WM-AES, the emitted signal must be large enough that the increase in intensity can be differentiated from the background continuum noise. The intensity and origin of the continua are drastically different for the two methods. In the case of WMCS-AAS, the most intense continuum source available is used, while, for WM-AES, the background continuum is several orders of magnitude less intense, arising from the sample matrix, stray light, and (in the case of carbon furnace emission) black body emission. In addition, electronic noise and photomultiplier tube dark current noise will appear at all wavelengths, and appear as background continua sources due to the wavelength modulation process. In general, however, the first three sources are of primary importance for WM-AES.

Snelleman (*1*) expressed the mean number of photoelectrons, $\bar{n}$, released at the photocathode per second for a continuum source as the product of the mean number of photons emitted by a black body, at the appropriate wavelength and temperature, and the luminosity of the monochromator. Simplifying this expression to show only those factors related to the monochromator

$$\bar{n} = K_1(H/F)DAt(\Delta\lambda)^2 \quad (1)$$

where K_1 is the combination of all nonmonochromator factors, H is the slit height, F is the focal length of the collimator of the monochromator, D is the angular dispersion, t is the dimensionless transmission factor of the internal optical components, and $\Delta\lambda$ is the effective width of the transmitted spectral interval (the spectral band-pass). The statistical noise, Δn, arising from this photoelectron flux is

$$\Delta n = K_2\,\Delta\lambda\,[(H/F)DAt]^{1/2} \quad (2)$$

where K_2 includes all the nonmonochromator factors.

Snelleman derived the detection limit, N_{min}, in terms of the relevant properties of the flame, the spectral line, the primary source, the monochromator, and the detection system. Simplifying this equation to show only the monochromator parameters yields

$$N_{min} = K_3\,[(H/F)DAt]^{-1/2} \quad (3)$$

As defined by Snelleman, N_{min} is the detection limit in terms of the number of atoms per cm^3 in the flame when the absorption signal is equal to Δn. Snelleman's detection limit can be related to the IUPAC detection limit (the concentration in solution which produces a signal three times the standard deviation of the base line) (*20*) by appropriate proportionality constants which can be included in K_3 with the other non-

monochromator factors. Consequently, N_{min} will be referred to as the detection limit in this study.

Equations 2 and 3 are based on two major assumptions. First, the wavelength modulation occurs at a high enough frequency that the fluctuation noise is insignificant and statistical noise is dominant. Thus eq 2 is proportional to the square root of eq 1. Second, a medium resolution monochromator is being used; the spectral band-pass of the monochromator is much greater than the half width of the absorption profile. This assumption leads to the derivation of eq 3 and accounts for the cancellation of the $\Delta\lambda$ term (eq 2) when the absorption signal is equated to Δn. The significance of both assumptions will be considered in more practical terms later in the paper.

The detection limit for WM-AES occurs when the emitted intensity equals the statistical noise, Δn. The mean number of photoelectrons, released at the photocathode per second by an emission line source, n_{em}, is given by Snelleman as

$$\bar{n}_{em} = N \exp[-E/kT] A_{21} \frac{q\omega}{Q4\pi} tHWLn \qquad (4)$$

where the variables have been defined in the original text. This expression, in terms of factors related to the monochromator, becomes

$$\bar{n}_{em} = NK_4 \omega t HW \qquad (5)$$

where N is the number of atoms per cm^3 in the flame, W is the slit width, and ω is the aperture in steradians. Since

$$W = DF(\Delta\lambda)$$

and

$$\omega = A/F^2$$

then

$$\bar{n}_{em} = NK_4\, \Delta\lambda[(H/F)DAt] \qquad (6)$$

where K_4 combines all the nonmonochromator parameters. The lowest detectable concentration of atoms, N_{min}, occurs at

$$\bar{n}_{em} = \Delta n \qquad (7)$$

The substitution of eq 2 and 5 into 6 gives

$$N_{min} = K_5\, [(H/F)DAt]^{-1/2} \qquad (8)$$

Equation 8 is identical with eq 3, with the exception of the proportionality constants. As a result, the dependence of the detection limit on the monochromator parameters is the same for WMCS-AAS and WM-AES. For both methods, the monochromator providing the best detection limit can be selected from the manufacturer's specifications. A comparison between WMCS-AAS and WM-AES cannot be made unless K_3 and K_5 are evaluated. Such an undertaking is beyond the scope of this paper.

WMCS-AAS

In Table I, the optical characteristics have been listed for a variety of monochromators which have been listed in order of increasing reciprocal linear dispersion (RLD). In addition to the manufacturer's specifications, D and $\Delta\lambda$ have been computed (from standard monochromator equations) as well as $\bar{n}$ and N_{min} (from eq 3 and 2, respectively). Since only the monochromator parameters are of interest in this study, the proportionality constants K_1 and K_3 have not been evaluated. Consequently, the photoelectron flux and the detection limit are expressed in units of nm mm^2 and nm mm^{-2}, respectively. mm^{-2}. Three different listings (covering the 200 nm to 600 nm range) are provided for the Spectraspan III, an echelle monochromator, since the dispersion varies systematically with each of the 85 orders employed.

Table I. Computed Minimum Detectable Signal and Photon Flux for Assorted Spectrometers

monochromator	F focal length, mm	A grating dimensions (mm × mm)	grooves mm^{-1}	D angular dispersion, deg nm^{-1}	RLD reciprocal linear dispersion, nm mm^{-1}	$\Delta\lambda^a$ spectral band-pass, nm	$10^6\bar{n}^b$ photoelectron flux, nm mm^2	$N_{min}{}^b$ detection limit, nm mm^{-2}
Spectraspan III[c]								
214 nm	750	46 × 96	79	0.021	0.063	0.0019	0.22	4.0
325 nm	750	46 × 96	79	0.014	0.095	0.0033	0.46	4.9
589 nm	750	46 × 96	79	0.0077	0.17	0.0068	1.0	6.6
THR 1500[d]	3000	80 × 110	2400	0.0025	0.13	0.0032	0.39	5.2
HR 1500[d]	1500	110 × 110	2400	0.0025	0.26	0.0065	4.3	3.2
HR 1000[d]	1000	120 × 140	2400	0.0025	0.4	0.010	21	2.2
HRS 0.6[d]	600	110 × 110	2400	0.0025	0.6	0.015	57	2.0
SPEX 1704[e]	1000	102 × 102	1200	0.0012	0.8	0.020	25	4.0
ATOMSCAN 2000[f]	750	75 × 95	1200	0.0012	1.0	0.025	36	4.2
270[g]	350	48 × 48	2400	0.0025	1.0	0.025	51	3.5
GM 252[h]	250	66 × 66	1180	0.0012	3.3	0.082	702	3.1
275[g]	200	40 × 45	1200	0.0012	4.0	0.10	540	4.3
JY-H.10[d]	100	30 × 30	1200	0.0012	8.0	0.20	2160	4.3

[a] Slit width normalized to 0.025 mm. [b] Slit height of 0.5 mm for the echelle, 5 mm for all others. [c] Spectrametrics, Inc., Andover, MA. [d] Instruments SA, Inc., Metuchen, NJ. [e] Spex Industries, Metuchen, NJ. [f] Fisher Scientific Co., Waltham, MA. [g] McPherson, Acton, MA. [h] Kratos Analytical Instruments, Westwood, NJ.

The detection limits and the photoelectron flux were computed assuming (1) t was the same for all the monochromators, (2) the effective area of illumination of the grating was equivalent to the grating area (except for the Spectraspan III, for which the effective area was computed), (3) slit widths were normalized to 0.025 nm, (4) 5-mm slit heights were used (except for the Spectraspan III for which 0.5-mm slit heights were used), and (5) first-order operation was used (except for the Spectraspan III). The optical transmission factor, t, varies according to the number and quality of the internal optical components of the monochromator. t reflects any light losses due to absorption, reflection, diffusion, and diffraction. For most monochromators, t is only a little less than 1 (*21*). Previous work (*22*) has shown that the luminosity of the Spectraspan III and a 0.5-m Ebert monochromator (Model 82-000, Jarrell-Ash Corp., Waltham, MA) are the same (within experimental error). Consequently, t has been assumed equivalent to 1 for all the monochromators considered in this study.

The effective area of illumination of the grating, the area of the grating perpendicular to the incident beam, can be determined as the product of the area of the grating and cos θ, where θ is the deviation of the grating from an angle perpendicular to the incident light. For conventional monochromators used in the first order, θ will be close to the blaze angle. The blaze angles, for the monochromators (with nonholographical gratings) in Table I ranged from 8.6° to 18.9°. Thus cos θ falls between 0.984 and 0.946 and the grating area is a reasonable approximation of the effective area of illumination. For the Spectraspan III, however, the blaze angle is 63° 26′ and cos θ is 0.447. Consequently, the computed effective area of illumination of the grating was used in Table I for the echelle monochromator.

The computed photon flux was normalized to 0.025-nm slit widths in Table I since the detection limit is independent of the slit width (eq 3). For most monochromators a wide selection of slit heights is available. In the case of line source AAS, the image size of the hollow cathode lamp is usually limiting. With graphite furnace atomization, the slit height cannot exceed the inside diameter for the tube. The hollow cathode lamp image size and the furnace tube diameter vary according to manufacturer. For this study, a slit height of 5 mm and a tube diameter of 6 mm were assumed, except for the echelle monochromator, where the slit height of 0.5 mm was used; 0.5 mm is the maximum slit height available on the echelle and is dictated by the dispersion of the prism.

The data listed in Table I show that the detection limits for every monochromator are comparable or slightly better than those computed for the echelle monochromator, the spectrometer generally used for WMCS-AAS. This is primarily a result of the decreased grating area and slit height of the echelle. Increasing the slit height and effective grating area by factors of 10 and 2, respectively, would increase the photoelectron flux by a factor of 20 and would improve the detection limit by $20^{1/2}$, or approximately 4.5. If such increases were possible for the echelle, the detection limit would be comparable to the best values of the other monochromators.

There are deviations from each of Snelleman's two basic assumptions which have not been taken into account which result in detection limits poorer than those predicted in Table I (*19*). First, the relative fluctuation noise component increases as the slit aperture is opened causing a deviation from the assumed statistical noise limited condition. As larger slit widths and heights are used, the photoelectron current increases, the fluctuation noise component becomes dominant (*19*), and a higher modulation frequency is necessary to maintain the statistical noise limited condition. However, wavelength modulating devices currently in use are not effective above 60 Hz (*23*, *24*). As a result, there is a critical photoelectron current above which the shot noise limited condition does not exist and the predicted detection limits of Table I are no longer valid.

Table II. Computed $\bar{n}$ (10^6 nm mm^2) as a Function of Slit Height and Width for the Echelle Polychromator at 324.7 nm

	$\bar{n}$					
	slit width shot noise limited			slit width fluctuation noise limited		
slit height, μm	25 μm	50 μm	100 μm	100 μm	200 μm	500 μm
100	0.20	0.66	2.4		9.2	55
200	0.40	1.3		4.8	18	110
300	0.60	2.0		7.2	28	160
500	1.0	3.3		12	46	280

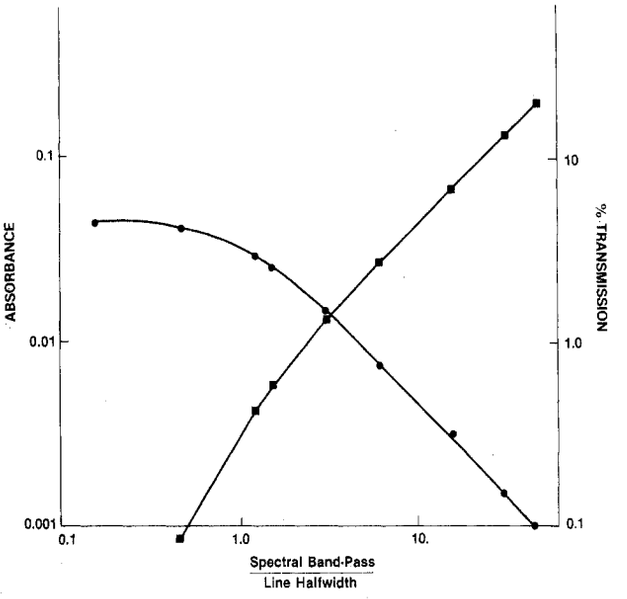

Figure 1. Computed absorbance (●) and absorption (■) as a function of the spectral band-pass–line half width ratio (*23*).

In Table II, $\bar{n}$ has been computed for the echelle monochromator at the Cu resonance wavelength (324.7 nm) using the theoretical bandwidths. The two 100 μm columns represent the transition boundary between the statistical noise and fluctuation noise limited cases, which was determined experimentally (*19*). It can be seen that, for a photon flux greater than approximately 4.0×10^{-6} nm mm^2, fluctuation noise dominates.

Table I lists the computed photoelectron flux for each of the monochromators. In general, while the detection limits are fairly uniform, the photoelectron flux increases dramatically with the increasing RLD. With the exception of the Spectraspan III and the THR 1500, every monochromator is fluctuation noise limited.

The second deviation from Snelleman's assumptions occurs when the band-passes of the high-resolution monochromators approach the half width of the absorption profiles. For a medium resolution monochromator, the spectral band-pass is much larger than the absorption profile half width. The absorption signal (measured at the photomultiplier tube) is a convolution of the absorption profile and the slit function. Thus the absorption signal will vary directly with the slit width while the absorbance changes inversely. As the spectral band-pass approaches the half width of the absorption profile, the absorption decreases at a faster rate while the absorbance asymptotically approaches a maximum. This is shown clearly in Figure 1, which was computed from the equations of de

Table III. Computed Minimum Detectable Signal and Photon Flux for Optimized Slit Parameters

monochromator	W slit width, mm	$\Delta\lambda$ spectral band-pass, nm	H slit height, mm	$10^6\overline{n}$ photoelectron flux, nm mm^2	N_{min} detection limit, nm mm^{-2}
Spectraspan (325 nm)	0.050	0.0057	0.5	1.3	4.9
THR 1500	0.042	0.0054	5.0	1.1	5.2
HR 1500	0.021	0.0054	5.0	2.9	3.2
HR 1000	0.014	0.0054	3.3	4.0	2.7
HRS 0.6	0.010	0.0060	2.2	4.0	3.0
SPEX 1704	0.010	0.0080	5.0	4.0	4.0
ATOMSCAN 2000	0.010	0.010	3.5	4.0	5.0
270	0.010	0.010	2.4	4.0	5.0
GM 252	0.010	0.033	0.18	4.0	16
275	0.010	0.040	0.23	4.0	20
JY-H.10	0.010	0.080	0.058	4.0	40

Table IV. Modulation Interval for the Low- and Medium-Resolution Monochromators

monochromator	slit width, mm	spectral band-pass, nm	modulation interval, nm
HRS 0.6	0.010	0.0060	0.024
SPEX 1704	0.010	0.0080	0.032
ATOMSCAN 2000	0.010	0.010	0.040
270	0.010	0.010	0.040
GM 252	0.010	0.033	0.13
275	0.010	0.040	0.16
JY-H.10	0.010	0.080	0.32

Galan and Winefordner (*25*). When the spectral band-pass profile half width ratio is 3.2, the absorbance signal is 95% of the expected value from a linear extrapolation. As the ratio decreases, the deviation increases. Consequently, the critical spectral band-pass is approximately three times the profile half width. Below this ratio Snelleman's assumption of a medium resolution monochromator and the computed detection limits are no longer valid. Since the absorption profile width varies roughly with wavelength, the minimum allowable spectral band-pass is wavelength dependent.

Table III lists revised detection limits for the monochromators in Table I. In Table III the slit parameters have been altered to ensure adherence to Snelleman's model. First, slit widths were selected for the high-resolution monochromators to obtain a spectral band-pass three times the absorption profile half width. For this comparison, the 324.7-nm Cu line was selected with an absorption half width of 0.0018 nm (*26*). Second, the slit widths and heights were reduced for the low- and medium-resolution monochromators until a photoelectron flux of 4.0×10^{-6} nm mm^{-2} was obtained. Slit widths were reduced first (since the detection limit is independent of the band-pass) to either the width providing a band-pass three times the absorption profile half width or a minimum of 0.010 nm. Slit widths smaller than 0.010 nm are not recommended because of the lack of accuracy and reproducibility of the settings and the distortion which may arise from the narrow widths. Slit heights were then reduced as necessary to reduce the photoelectron flux to 4.0×10^{-6} nm mm^{-2}.

The monochromators with RLDs of 1.0 nm/mm or less gave detection limits that ranged from comparable to a factor of 1.8 better than that of the echelle monochromator. The detection limits for the monochromators with high (>1.0 nm/mm) RLDs were considerably poorer than the rest.

WM-AES

The detection limits listed in Table I can be applied directly to WM-AES. There is no concern about the photoelectron flux being too high for the low- and medium-resolution monochromators, since the background emission continuum for WM-AES is many orders of magnitude less intense than the WMCS-AAS source. The slit widths of the monochromators with low RLDs must be increased to obtain a spectral band-pass three times the half width of the emission profile (usually about the same half width as the absorption profile), but the photoelectron flux will still be in the statistical noise limited range.

From a practical point of view, it is desirable to decrease the spectral band-pass of the monochromators with high RLDs to reduce the possibility of structured background interferences. With a band-pass 1 to 2 orders of magnitude greater than the absorption or emission profile, the *center* of the spectral band-pass must be offset to both sides (during the modulation process) by a distance equivalent to one band-pass to make a reference measurement (no contribution from the analytical signal). Thus, any structure falling within two band-pass distances on either side of the profile center can produce an interference. In Table IV, the modulation interval (four times the spectral band-pass) is given for the low- and medium-resolution monochromators using a slit width of 0.010 mm. To put this wavelength interval in perspective, the Perkin-Elmer Corp. (*27*), recommends the use of spectral band-passes of 0.2 nm or 0.7 nm for routine determinations. Thus, the larger band-passes of the monochromators with high RLDs do increase the risk of structured background interferences, but this risk does not appear significantly greater than that encountered for conventional AAS.

The computed detection limits in Table I predict that any of the monochromators would be satisfactory for WM-AES. The best and worst detection limits are only different by a factor of 2. The prices, however, vary by a much larger factor. Consequently, it would appear that the low-resolution monochromators are preferable for WM-AES, from cost considerations.

LITERATURE CITED

(1) Snelleman, W. *Spectrochim. Acta, Part B* **1968**, *23B*, 403.
(2) Nitis, G. J.; Svoboda, V.; Winefordner, J. D. *Spectrochim. Acta, Part B* **1972**, *27B*, 345.
(3) Veillon, C.; Merchant, P. *Appl. Spectrosc.* **1973**, *27*, 361.
(4) Zander, A. T.; O'Haver, T. C.; Keliher, P. N. *Anal. Chem.* **1976**, *48*, 1166.
(5) Zander, A. T.; O'Haver, T. C.; Keliher, P. N. *Anal. Chem.* **1977**, *49*, 838.
(6) Harnly, J. M.; O'Haver, T. C. *Anal. Chem.* **1977**, *49*, 2187.
(7) Epstein, M. S.; Zander, A. T. *Anal. Chem.* **1979**, *51*, 915.
(8) Snelleman, W.; Rains, T. C.; Yu, K. W.; Cook, H. D.; Menis, O. *Anal. Chem.* **1970**, *42*, 394.
(9) Maines, I. S.; Mitchell, D. G.; Rankin, J. M.; Bailey, B. W. *Spectrosc. Lett.* **1972**, *5*, 251.
(10) Rains, T. C.; Menis, O. *Anal. Lett.* **1974**, *7*, 715.
(11) Epstein, M. S.; O'Haver, T. C. *Spectrochim. Acta, Part B* **1975**, *30B*, 135.
(12) Epstein, M. S.; Rains, T. C.; O'Haver, T. C. *Appl. Spectrosc.* **1976**, *30*, 324.
(13) Epstein, M. S.; Rains, T. C.; Brady, T. J.; Moody, J. R.; Barnes, I. L. *Anal. Chem.* **1978**, *50*, 874.
(14) Ottaway, J. M.; Hutton, R. C.; Littlejohn, D.; Shaw, F. *Wiss. Z.—Karl-Marx-Univ., Leipzig, Math.-Naturwiss. Reihe* **1979**, *28*, 357.

(15) Ottaway, J. M.; Bezur, L.; Marshall, J. *Analyst (London)* **1980**, *105*, 1130.
(16) Harnly, J. M.; O'Haver, T. C.; Golden, B. M.; Wolf, W. R. *Anal. Chem.* **1979**, *51*, 2007.
(17) Harnly, J. M.; O'Haver, T. C. *Anal. Chem.* **1981**, *53*, 1291.
(18) Marshall, J.; Littlejohn, D.; Ottaway, J. M.; Harnly, J. M.; Miller-Ihli, N. J.; O'Haver, T. C. *Analyst (London)* **1983**, *108*, 178.
(19) Harnly, J. M. *Anal. Chem.* **1982**, *54*, 1043.
(20) IUPAC Commission on Spectrochemical and Other Optical Procedures, Nomenclature, Symbols, Units, and Their Usage in Spectrochemical Analysis. II Data Interpretation *Pure Appl. Chem.* **1976**, *45*, 99.
(21) Herrmann, R.; Alkemade, C. T. J. "Chemical Analysis by Flame Photometry"; Interscience: New York, 1963; p 130.
(22) O'Haver, T. C.; Harnly, J. M.; Zander, A. T. *Anal. Chem.* **1978**, *50*, 1221.
(23) Harnly, J. M. *Anal. Chem.* **1982**, *54*, 876.
(24) Bezur, L.; Marshall, J.; Ottaway, J. M.; Fakhrul-Aldeen, R. *Analyst (London)* **1983**, *108*, 553.
(25) de Galan, L.; Winefordner, J. D. *Spectrochim. Acta, Part B* **1968**, *23B*, 277.
(26) Kelliher, P. N.; Wohlers, C. C. *Anal. Chem.* **1974**, *46*, 682.
(27) "Analytical Methods for Atomic Absorption Spectrophotometry"; Perkin-Elmer Corp.: Norwalk, CT, Jan 1982.

RECEIVED for review June 2, 1983. Resubmitted November 23, 1983. Accepted January 19, 1984. Mention of trademark or proprietary products does not constitute a guarantee or warranty of the product by the U.S. Department of Agriculture and does not imply their approval to the exclusion of other products that may also be suitable.

Comparison of Pneumatic Nebulizers in Current Use for Inductively Coupled Plasma Atomic Emission Spectrometry

Frans J. M. J. Maessen,* Pieter Coevert, and Johannes Balke

Laboratory of Analytical Chemistry, University of Amsterdam, Nieuwe Achtergracht 166, 1018 WV Amsterdam, The Netherlands

Two concentric and three cross-flow nebulizers operated with and without a pump are examined. The nebulization systems are primarily assessed on the basis of their suitability for simultaneous multielement analysis, considering the signal-to-background ratio (S/B) as a principal analytical parameter and the pressure drop of the nebulizing gas across the gas capillary (ΔP) as the principal experimental variable. The relations between ΔP and S/B have been established at 14 analysis wavelengths. Compared to natural liquid uptake, forced nebulizer feeding leads to less pronounced peaks in the ΔP vs. S/B curves. The transport efficiency (ϵ) measured by direct aerosol collection is determined as a function of the flow rate of the nebulizing gas (Q_G) over ranges of Q_G of specific interest for the individual nebulizers. The moderate variability of analytical performance observed for the nebulizers examined is discussed on the basis of the applicable values of ϵ, Q_L, and Q_G.

Over the last few years, papers regularly appeared dealing with the performance of nebulizers for ICP analysis (*1–9*). In these studies the efficiency of the nebulizing process was established either indirectly by measuring the difference between the uptake and waste (*1–5*) or directly by determining the increase of weight of adsorption columns connected in series to the plasma exit of the spray chamber (*6–9*). Since the aerosol concentration in the plasma can be calculated only if the efficiency of the nebulization process is known, accurate determination of the latter quantity is of the utmost importance for assessing nebulizer–spray chamber performance. Smith and Browner (*10*) recently examined the relative merits of several direct and indirect methods for determining the nebulization efficiency or, better, the transport efficiency, as defined by the authors. Their results showed that the indirect method is prone to severe systematic and random error whereas of the considered direct methods, viz., filter, cascade impact, and adsorption by silica gel, the silica gel collection method appeared to be affected with positive bias. However, for low gas flow systems, such as the nebulizer described by Ripson and De Galan (*7*), this bias might be small enough to make results from solvent adsorption procedures acceptable as an indication of system performance (*11*, *12*). But only efficiencies based on solute transport measurements, e.g., cascade impact or filter system, should be adequate to allow meaningful interlaboratory comparison of transport efficiency data (*10*).

Starting from this conclusion and considering the large variety of nebulizers presently available for ICP analysis (*13*), a study was undertaken to contribute to the performance evaluation of various types of nebulizers and to facilitate nebulizer selection in analytical practice.

In the present work five pneumatic nebulizers were examined, viz., two concentric, two cross-flow, and one Babington type. The concentric and cross-flow nebulizers were operated with both free and forced feeding. Transport efficiencies were measured employing an aerosol collection system using filters. Line and background measurements were performed at 14 analysis wavelengths. The nebulization systems examined were primarily assessed on the basis of their suitability for simultaneous multielement analysis, considering the signal-to-background ratio as a principal analytical parameter (*14–16*). The pressure drop of the nebulizing gas across the gas capillary (ΔP) was considered as the principal experimental variable because in commercial ICP instruments ΔP is frequently the only precisely controllable nebulizer parameter and, further, because ΔP is a fundamental parameter for nebulizer modification, e.g., the high-pressure "MAK" nebulizer (*17*), and nebulizer design (*18*), including the calculation of nozzle shapes (*19*).

EXPERIMENTAL SECTION

Nebulizer Types. The following nebulizers were tested. Two concentric glass nebulizers, Models TR-20-B1 and TR-30-B1, from J. E. Meinhard Associates, Santa Ana, CA (*20*), and three cross-flow nebulizers, viz., one adjustable, one fixed, and one of the high solids type, all three from Jarrell-Ash, Waltham, MA. The adjustable cross-flow nebulizer (Catalog No. 90-974) is essentially the same as the pneumatic nebulizer developed by Knisely et al. (*21*) for use at low gas flow rates. The fixed cross-flow nebulizer (Catalog No. 90-790) is based on the design

0003-2700/84/0356-0899$01.50/0